Journal of Nondestructive Evaluation, Vol. 1, No. 1, 1980

Methods for Determining the Depth of Near-Surface Defects

Dixon Cleveland,[1] Andrew R. Barron,[1] and Anthony N. Mucciardi[1]

Received November 5, 1979

In previous work by the authors,[1,6] it was demonstrated that the presence of near-surface defects could be detected reliably, even though the defect echo was contained within the near-surface echo. The algorithm consists of examining the variation in the composite (near-surface plus defect) response after it has been deconvolved from a near-surface response known to be defect-free. This paper presents two algorithms that have been developed subsequent to the work presented in ref. (6) for estimating the *depth* of a near-surface defect, given that its presence has already been detected. One algorithm uses complex frequency domain techniques, and the other uses time domain analysis. Both procedures operate on the surface-plus-defect signal, using reference signals containing surface-only and defect-only responses. The defect signal is extracted from the composite signal. Defect depth is then computed from the time difference between the centers of the front-surface and extracted defect responses. A mean absolute depth error of 0.015 in. was obtained by applying the algorithms to experimental data containing depths from 0.020 to 0.130 in. below the near-surface.

KEY WORDS: ultrasonics; surface defects; defect depth; deconvolution; correlation; NDE.

INTRODUCTION

A common ultrasonic method for measuring the depth of a defect in metal is to insonify the defect with a pulsed transducer in the longitudinal mode and aligned perpendicular to the surface of the test piece, and to compute the distance between the surface and the defect from the time difference between the surface and defect responses. When observing a very shallow defect, however, the front surface response overlaps significantly the response from the defect, and it becomes impractical to estimate the occurrence times of the surface and defect signals by peak detection.

[1]Adaptronics, Inc., Westgate Research Park, 1750 Old Meadow Road, McLean, Virginia 22102.

In previous work by Adaptronics,[1, 2, 5, 6] it was demonstrated that the presence of near-surface defects could be *detected* reliably. The algorithm developed is as follows. The power spectrum of the test signal's front surface response is divided (deconvolved) by the power spectrum of a reference front surface response taken with the same transducer on a section of the same type of material known to have no near-surface defect. If the test piece has no defect, the front surface power spectrum will resemble closely that of the reference, and the deconvolved spectrum will approach unity for all frequencies. If a defect is present, a significant variation from unity appears. If the variance of the deconvolved spectrum exceeds a threshold, a defect is detected. In the following derivations, it is desired to estimate the *depth* of the near-surface defect, given that its presence has already been detected.

0195-9298/80/0300-0021$03.00/0

DEFINITION OF NEAR-SURFACE DEFECTS

With the transducers used in this work, the time width T_w of the front surface responses, as measured between the points where the amplitude reached 10% of its maximum, is approximately

$$T_w = 1.2\ \mu s \tag{1}$$

Given a longitudinal wave velocity in stainless steel,

$$v = 0.22\ \text{in.}/\mu s \tag{2}$$

and a roundtrip length l equal to twice the defect depth δ,

$$l = 2\delta \tag{3}$$

the minimum depth $\delta_{\min}$, for which there is adequate time separation between the surface and defect responses, is given by

$$T_w = \frac{l}{v} = \frac{2\delta_{\min}}{v} \tag{4}$$

or

$$\delta_{\min} = \frac{vT_w}{2} = 0.13\ \text{in.} \tag{5}$$

Near-surface defects are defined in this work to be those less than 0.13 in. deep.

A NEAR-SURFACE DEFECT MODEL

Two approaches are developed here for estimating the depth of a near-surface defect. [Other work can be found in refs. (4, 8, 9), for example.] One uses complex frequency domain techniques, and the other uses time domain analysis. Both procedures operate on the surface-plus-defect signal, using reference signals containing surface-only and defect-only responses. First, $s(t)$ is defined as the front surface time response from the piece under test, $d(t)$ is the defect response, and $x(t)$ is the surface-plus-defect response. Only $x(t)$ is measurable directly because $s(t)$ and $d(t)$ are merged within each other.

Given a reference block with a defect of known size, orientation, and depth greater than 0.13 in., a reference surface signal $s_r(t)$ and a reference defect signal $d_r(t)$ are obtained with the same transducer as used with the test piece. Ideally, the reference defect would approximate a point source, for the same reasons discussed in ref. (9). A small, one-half inch deep, flat-bottom hole, such as shown in Fig. 1, would serve well for this purpose. The reference signals $s_r(t)$ and $d_r(t)$ are time shifted such that their centers, as determined by an appropriate signal-center location algorithm, occur at $t=0$ (Fig. 1). The objective of the following derivation is to obtain an estimate of defect depth, given $x(t)$, $s_r(t)$, and $d_r(t)$.

It is assumed that the superposition principle holds for ultrasonic waves and thus that the surface-plus-defect response is equal to the sum of the surface and defect responses:

$$x(t) = s(t) + d(t) \tag{6}$$

It is further assumed that the surface responses from the test and reference pieces are nearly identical and that the defect responses from the test and reference pieces strongly resemble each other. The differences between the respective signals are primarily amplitude variation and time shifting:

$$s(t) \simeq a_s s_r(t - t_s) \tag{7}$$

and

$$d(t) \simeq a_d d_r(t - t_d) \tag{8}$$

where the a_s and a_d are the amplitude scale factors and t_s and t_d are the time shift parameters for the surface and defect signals. Since ultrasonic signals are generally amplified to give full-scale voltages for the front surface responses, the magnitudes of $s(t)$ and $s_r(t)$ will be about the same, and a_s will therefore be approximately unity. The defect scale factor a_d will generally indicate the relative reflectivity of the test defect as compared to the reference defect.

By substitution of Approximations (7) and (8) into Eq. (6), a model of the test signal $x(t)$ may be constructed from the reference responses:

$$x(t) \simeq a_s s_r(t - t_s) + a_d d_r(t - t_d) \tag{9}$$

The objective in the model solution is to obtain estimates of the four parameters a_s, a_d, t_s, and t_d, and from the t's the depth can be found. Complex Fourier transforms are obtained from the three measurable time signals:

$$X(f) \leftarrow x(t) \tag{10}$$

$$S_r(f) \leftarrow s_r(t) \tag{11}$$

$$D_r(f) \leftarrow d_r(t) \tag{12}$$

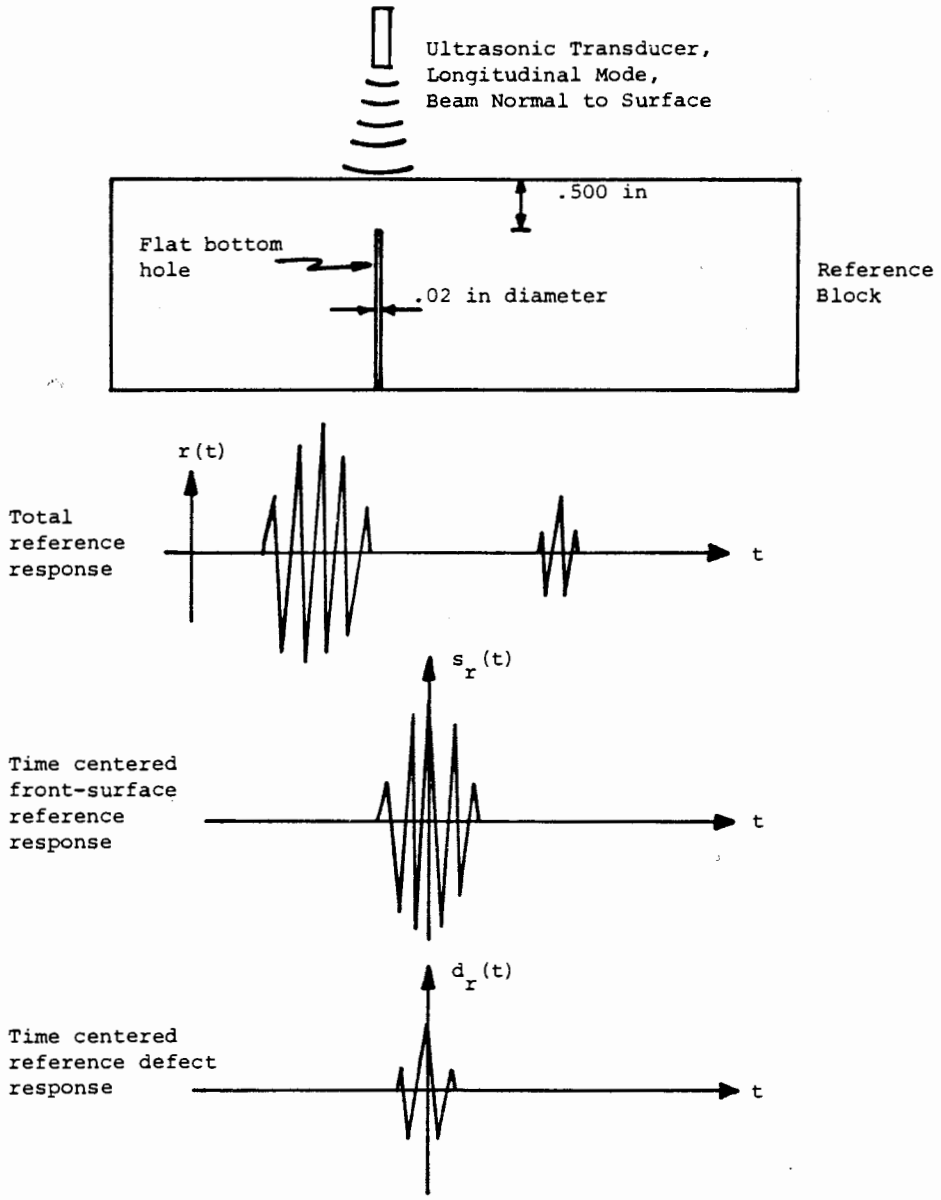

Fig. 1. Reference block and resulting transducer reference time waveforms to be used for near-surface defect depth estimation.

Taking the transform of Approximation (9) and invoking linearity and the time shift operator on the two terms of the right-hand side yields

$$X(f) \simeq a_s e^{-j2\pi f t_s} S_r(f) + a_d e^{-j2\pi f t_d} D_r(f) \quad (13)$$

Since the amplitude of the defect response is small by comparison to the front surface response, the surface parameters a_s and t_s are estimated first. Equation (13) is divided through (or deconvolved) by $S_r(f)$:

$$\frac{X(f)}{S_r(f)} \triangleq Z_s(f) \simeq a_s e^{-j2\pi f t_s} + a_d e^{-j2\pi f t_d} \frac{D(f)}{S_r(f)} \quad (14)$$

For convenience, the ratio $X(f)/S_r(f)$ is defined as $Z_s(f)$. Because the magnitude of the defect (second) term is small with respect to the surface

(first) term, it is treated as if it were noise. Estimates for a_s and t_s are found by ignoring the defect term and equating separately the magnitude and phase portions of Approximation (14):

$$|Z_s(f)| \simeq a_s \tag{15}$$

and

$$\measuredangle[Z_s(f)] \triangleq \phi_s(f) \simeq -2\pi f t_s \tag{16}$$

The angle of $Z_s(f)$ is defined as $\phi_s(f)$. The solution for the angle in Eq. (16) is complicated by the existence of multiple solutions ($\phi, \phi \pm 2\pi, \phi \pm 4\pi, \ldots$). A large portion of any ambiguity is removed by differentiating $\phi_s(f)$ with respect to f to obtain

$$\frac{d[\phi_s(f)]}{df} \simeq -2\pi t_s \tag{17}$$

Since the Fourier transform is sampled at uniform intervals Δf, it is convenient to define

$$\Delta\phi_s(f) = \phi_s(f) - \phi_s(f - \Delta f) \tag{18}$$

in which case Eq. (17) becomes

$$-\frac{\Delta\phi_s(f)}{2\pi\Delta f} \simeq t_s \tag{19}$$

The differential angles in Eq. (19) are less ambiguous than the total angles of Eq. (16).

Equations (15) and (19) hold for all frequencies, so each complex frequency component of the Fourier transform yields a separate estimate for both the amplitude and phase parameters. The best overall surface parameter estimates $\hat{a}_s$ and $\hat{t}_s$ are *weighted averages* of the individual frequency estimates, where the averaging of the separate frequency estimates significantly reduces the effects of the "noise" from the defect term:

$$\hat{a}_s = \frac{\sum_f w_s(f)|Z_s(f)|}{\sum_f w_s(f)} \tag{20}$$

and

$$\hat{t}_s = \left(\frac{-1}{2\pi\Delta f}\right)\frac{\sum_f w_s(f)\Delta\phi_s(f)}{\sum_f w_s(f)} \tag{21}$$

The weights $w_s(f)$ are chosen to emphasize the individual estimates where the amplitudes of $S_r(f)$, which is the denominator in Eq. (14), are large and thus where the relative noise is small. Conversely, the weights de-emphasize points where $S_r(f)$ is small and where the relative noise is therefore high. The weighting function that yields a least-mean-square error for the surface amplitude scale factor $\hat{a}_s$ is

$$w_s(f) = |S_r(f)|^2 \tag{22}$$

Using these weights, the a_s and t_s estimates of Eq. (20) and (21) become

$$\hat{a}_s = \frac{\sum_f |S_r(f)|^2 |Z(f)|}{\sum_f |S_r(f)|^2} \tag{23}$$

and

$$\hat{t}_s = \left(\frac{-1}{2\pi\Delta f}\right)\frac{\sum_f |S_r(f)|^2 \Delta\phi_s(f)}{\sum_f |S_r(f)|^2} \tag{24}$$

It is important to note that division by zero, which may occur in the computation of $Z_s(f)$ if $\hat{a}_s$ is calculated from Eq. (20), will not occur if the weighting of Eq. (22) is used and $\hat{a}_s$ is calculated from Eq. (23).

Now given the surface parameter estimates $\hat{a}_s$ and $\hat{t}_s$, this data may be used in the near-surface defect model, Approximation (13), to obtain the defect parameter estimates $\hat{a}_d$ and $\hat{t}_d$. The front surface term is shifted to the left side, and the equation is divided through (deconvolved) by the defect reference spectrum $D_r(f)$:

$$\frac{X(f) - \hat{a}_s e^{-j2\pi f\hat{t}_s} S_r(f)}{D_r(f)} \triangleq Z_d(f) \simeq a_d e^{-j2\pi f t_d} \tag{25}$$

For convenience, the left-hand term is defined as $Z_d(f)$. The defect parameter estimates $\hat{a}_d$ and $\hat{t}_d$ are found from $Z_d(f)$, just as the surface parameter estimates were found from $Z_s(f)$:

$$\hat{a}_d = \frac{\sum_f w_d(f)|Z_d(f)|}{\sum_f w_d(f)} \tag{26}$$

and

$$\hat{t}_d=\left(\frac{-1}{2\pi\Delta f}\right)\frac{\sum_f w_d(f)\Delta\phi_d(f)}{\sum_f w_d(f)} \tag{27}$$

Since the denominator of $Z_d(f)$ in Eq. (25) is $D_r(f)$, the weighting function for a least-mean-square error on the defect amplitude scale factor $\hat{a}_d$ is

$$w_d(f)=|D_r(f)|^2 \tag{28}$$

and the $\hat{a}_d$ and $\hat{t}_d$ estimates of Eqs. (26) and (27) become

$$\hat{a}_d=\frac{\sum_f |D_r(f)|\,|X(f)-\hat{a}_s e^{-j2\pi f\hat{t}_s}S_r(f)|}{\sum_f |D_r(f)|^2} \tag{29}$$

and

$$\hat{t}_d=\left(\frac{-1}{2\pi\Delta f}\right)\frac{\sum_f |D_r(f)|^2\Delta\phi_d(f)}{\sum_f |D_r(f)|^2} \tag{30}$$

This completes the estimates of all four near-surface defect model parameters.

It is possible to obtain refined estimates of the four parameters by reiterating the solution. In the first iteration the front-surface parameters were estimated under the assumption that the defect term of Eq. (14) was totally noise. In the second iteration, the majority of that term may be subtracted out, based upon the first pass estimates of a_d and t_d, so the noise will be reduced and the surface parameters can be better estimated. With the improved surface parameter estimates, the defect parameter estimates can also be improved.

MODEL SOLUTION IN THE TIME DOMAIN

The time domain solution to the near-surface defect model of Eq. (9) involves first computing a weighted correlation function between $x(t)$ and $s_r(t)$ to time align the two signals:

$$C_s(\tau)=\sum_t w_{cs}(t)s_r(t)s(t-\tau) \tag{31}$$

The value of τ for which $C_s(\tau)$ is a maximum is the estimate $\hat{t}_s$:

$$\hat{t}_s=\tau \qquad [C_s(\tau)=\max] \tag{32}$$

While a constant weighting function would provide adequate results, it is known *a priori* (a) that any defect response would exist in the latter half of the front-surface response, and (b) that the front-surface response has a finite time. Therefore a weighting function should emphasize the first part of the surface response, deemphasize the regions where defect "noise" is known to exist, and deemphasize the regions where the front surface signal is known not to exist. Such a weighting function, shown in Fig. 2, is

$$w_{cs}(t)=1+\cos\left[\frac{\pi(t+T_0)}{T_{ws}}\right]$$

for $-T_{ws}-T_0\leqslant t\leqslant T_{ws}-T_0$, and

$$w_{cs}(t)=0, \quad \text{elsewhere} \tag{33}$$

where the width and offset times T_{ws} and T_0 were selected for this work based on the width T_w [Eq. (1)] of the typical front-surface responses:

$$T_{ws}=T_w/2=0.65\ \mu\text{s} \tag{34}$$

and

$$T_0=0.20\ \mu\text{s} \tag{35}$$

Once the reference front-surface signal $s_r(t)$ is time aligned with the test signal $x(t)$, $s_r(t)$ is amplitude scaled to match $x(t)$. The amplitude scale parameter a_s is derived from the model equation (9) by dividing through by $s_r(t-\hat{t}_s)$ and treating the defect term as noise:

$$a_s\simeq\frac{x(t)}{s_r(t-\hat{t}_s)} \tag{36}$$

Each time point gives an estimate of a_s, and the best overall estimate is a weighted sum:

$$\hat{a}_s=\frac{\sum_t w_s(t)\dfrac{x(t)}{s_r(t-\hat{t}_s)}}{\sum_t w_s(t)} \tag{37}$$

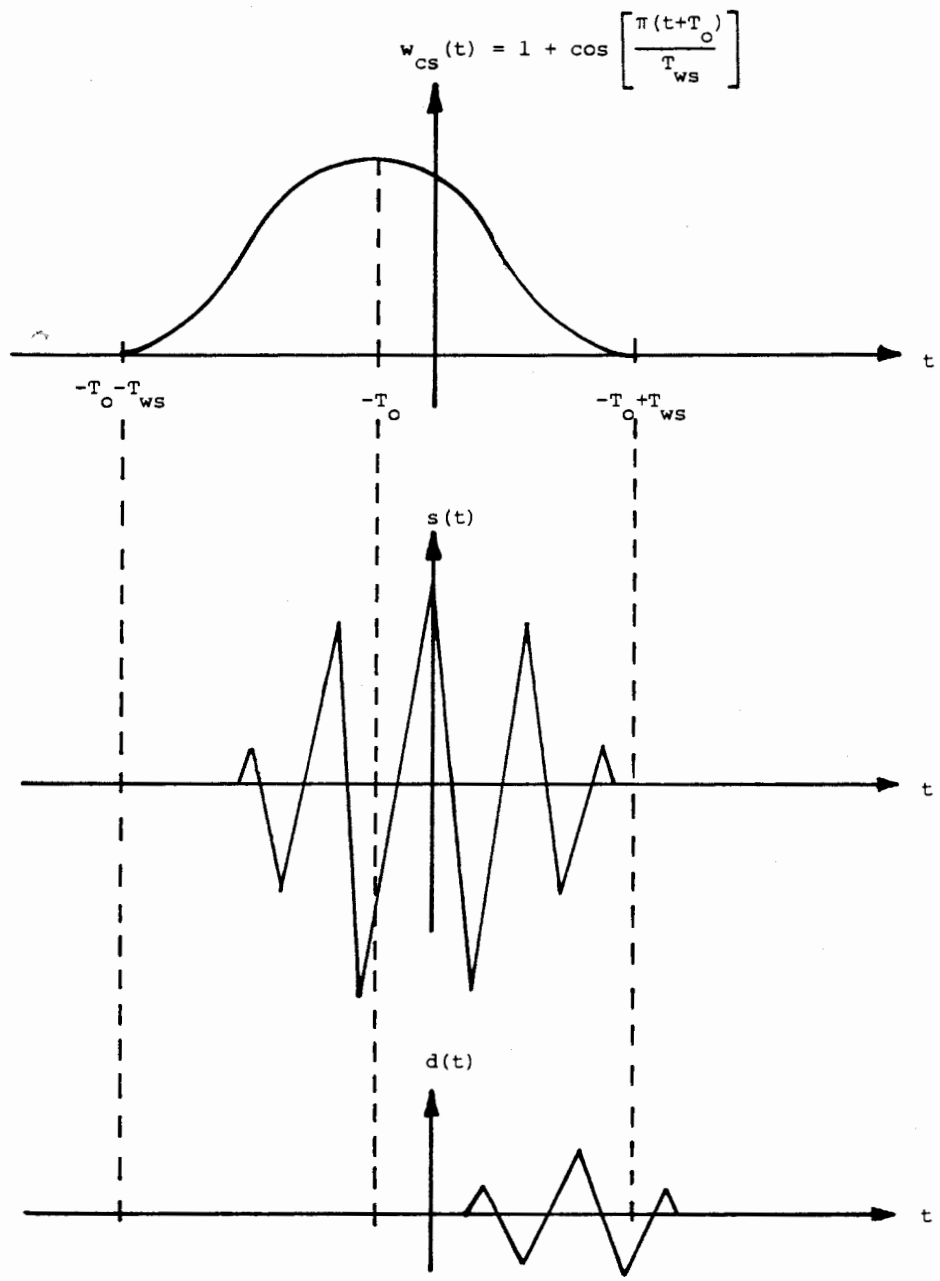

Fig. 2. Correlation weighting function for time alignment of front-surface reference with near-surface defect signal.

Since $s_r(t-\hat{t}_s)$ is in the denominator, a least-mean-square error weighting function is

$$w_s(t)=s_r^2(t-\hat{t}_s) \tag{38}$$

but for the same reasons that the cosine weighting was used in estimating the surface occurrence time t_s, it should be used here in estimating the surface amplitude a_s. Thus the overall weighting function becomes

$$w_s(t)=\left\{1-\cos\left[\frac{\pi(t+T_0)}{T_s}\right]\right\}s_r^2(t-\hat{t}_s) \tag{39}$$

Now the surface amplitude estimate $\hat{a}_s$ from Eqs.

(37) and (39) becomes

$$\hat{a}_s = \frac{\sum_{t=-T_s-T_0}^{T_s-T_0} \left\{1-\cos\left[\frac{\pi(t+T_0)}{T_s}\right]\right\} s_r(t-\hat{t}_s)x(t)}{\sum_{t=-T_s-T_0}^{T_s-T_0} \left\{1-\cos\left[\frac{\pi(t+T_0)}{T_s}\right]\right\} s_r^2(t-\hat{t}_s)} \tag{40}$$

Note that, in going from Eq. (37) to (39), the division by a possible zero in $s_r(t-\hat{t}_s)$ was eliminated.

Now given the surface parameters $\hat{t}_s$ and $\hat{a}_s$, the defect signal can be isolated. From the model equation (9), the front-surface signal is subtracted out, yielding a difference signal $d(t)$:

$$x(t)-\hat{a}_s s_r(t-\hat{t}_s) \triangleq d(t) \simeq a_d d_r(t-t_d) \tag{41}$$

Since the defect signal now stands alone, a peak detection or signal-center location algorithm may be used to estimate the defect occurrence time $\hat{t}_d$. A signal-center location algorithm is given in the Appendix.

If the residual noise from front surface subtraction is too large for peak detection or if the defect amplitude parameter $\hat{a}_d$ is desired, the defect time parameter $\hat{t}_d$ should be found using the correlation

$$C_d(\tau) = \sum_t w_{cd}(t) d_r(t) d(t-\tau) \tag{42}$$

where the defect correlation weights are again a cosine function, but this time with smaller width (to correspond to the shorter time responses of the defects) and no time offset:

$$\begin{aligned} w_{cd}(t) &= 1+\cos\left[\frac{\pi t}{T_{wd}}\right] && -T_{wd} \leqslant t \leqslant T_{wd} \\ w_{cd}(t) &= 0 && \text{elsewhere} \end{aligned} \tag{43}$$

where

$$T_{wd} = 0.30\ \mu\text{s} \tag{44}$$

The defect time estimate $\hat{t}_d$ is that time where the correlation function $C_d(\tau)$ is a maximum

$$\hat{t}_d = \tau \qquad [C_d(\tau) = \max] \tag{45}$$

The defect amplitude coefficient a_d is now solved from Eq. (41):

$$\frac{x(t)-\hat{a}_s s_r(t-\hat{t}_s)}{d_r(t-\hat{t}_d)} \triangleq z_r(t) \simeq a_d \tag{46}$$

and the best overall estimate is

$$\hat{a}_d = \frac{\sum_t w_d(t) z_r(t)}{\sum_t w_d(t)} \tag{47}$$

where

$$w_d(t) = \left\{1-\cos\left[\frac{\pi t}{T_{wd}}\right]\right\} d_r^2(t-\hat{t}_d) \tag{48}$$

which minimizes noise and provides the least-mean-square error estimate $\hat{a}_d$. Combining Eqs. (48) and (47) yields

$$\hat{a}_d = \frac{\sum_t \left\{1-\cos\left[\frac{\pi t}{T_{wd}}\right]\right\} d_r(t-\hat{t}_d)\{x(t)-\hat{a}_s s_r(t-\hat{t}_s)\}}{\sum_t \left\{1-\cos\left[\frac{\pi t}{T_{wd}}\right]\right\} d_r^2(t-\hat{t}_d)} \tag{49}$$

which completes the estimates of all four near-surface defect model parameters.

It is possible, as with the frequency domain solution, to obtain refined estimates of the four parameters by reiterating the solution. The front-surface parameters may be improved if a large percentage of the defect, which acts as noise, is eliminated. However, the weighting function of Eq. (33) is designed to reduce the defect noise *a priori*, so reiteration should not be necessary to obtain best results.

DEPTH ESTIMATE FROM MODEL PARAMETER ESTIMATES

Finally, the defect depth $\hat{\delta}$ is estimated from the difference between the occurrence times of the front-surface and defect signals:

$$\hat{\delta} = \frac{v(\hat{t}_d-\hat{t}_s)}{2} \tag{50}$$

Some information about the defect size may be inferred from the reflectivity coefficient $\hat{a}_d$ and knowledge of the reference defect.

ADVANTAGES OF THE TIME DOMAIN APPROACH

The time and frequency domain solutions to the model of Approximation (9) are analogous in many respects. The front-surface parameters are estimated first, while treating the defect response as noise, and then the defect parameters are estimated with the use of the front-surface parameters. Where complex division (deconvolution) is used in the frequency domain, correlation methods are used in the time domain.

The time domain solution has several advantages over the frequency domain solution:

1. The time domain solution does not require a reference defect signal. The time of defect occurrence can be determined from signal-center location algorithms (such as given in the Appendix), once the front-surface response is removed, eliminating the need for correlation against a reference defect.
2. *A priori* knowledge that the defect exists toward the right side of the front-surface response allows the use of a weighting function to minimize the impact of the defect signal in locating the front-surface occurrence time.
3. *A priori* knowledge that the front-surface and defect responses are limited in their time duration allows the use of a weighting function to minimize the impact of waveform noise outside the time window of the signal.
4. The time domain solution is more intuitive.

PRACTICAL APPLICATION OF THE THEORY

The front-surface response is quite repeatable; the human eye can easily and consistently distinguish one transducer from another and most of the characteristic shape features of the waveform remain much the same from shot to shot. However, in subtracting one front-surface response from another, in either the frequency or the time domains, the variations become significant because the magnitude of the difference is large with respect to the magnitude of the defect which is being sought.

It is believed that the major source of variation is due to amplifier saturation during the front-surface response. This conflicts with the initial model assumptions made above that the surface responses are identical. Thus after the front-surface response is subtracted out of the surface-plus-defect response, the defect is often still masked by the front-surface residual, and location of the defect through peak detection methods remains inadequate. For practical operation, it is recommended that the amplifier gain be reduced well below saturation for the detection and location of near-surface defects. Successive shots with higher gain may be used for analysis of the deeper regions of the material.

Despite the front-surface saturation, it was desirable to demonstrate the theory on experimental data, and the following method was developed to compensate for shot-to-shot variation. The reference front-surface response, for a given transducer and a given material, is redefined to be an average of several (in this work, four) individual front-surface responses. Also, the standard deviation of the several responses is computed. An example of the individual front-surface responses along with the average and standard deviation is shown in Fig. 3. The experimental data are described in ref. (1). Figure 4 shows the averages and standard deviations for transducers 1 and 2 on stainless steel and Inconel. It can be seen from the standard deviation curves that the greatest variations in front-surface responses occur when the transducer amplifier is coming out of saturation.

The average reference, after time alignment and amplitude matching with the test signal, is subtracted from the test signal. The resulting difference signal contains the defect signal and residual front-surface noise. The large majority of the front-surface noise, however, exists in the form of spikes, which occur where the standard deviation of the average reference is high. The method for reducing the noise is to attenuate the difference signal in proportion to the standard deviation. The fundamental notion is that those large magnitudes in the difference signal which occur where there is expected variation between front-surface responses should be ignored, and that the remaining signal constitutes the defect. Thus a modified difference signal $d'(t)$ is computed from $d(t)$ [see Eq. (41)]:

$$d'(t) = w_o(t)d(t) \tag{50}$$

where $w_o(t)$ is the system attenuation weight due to

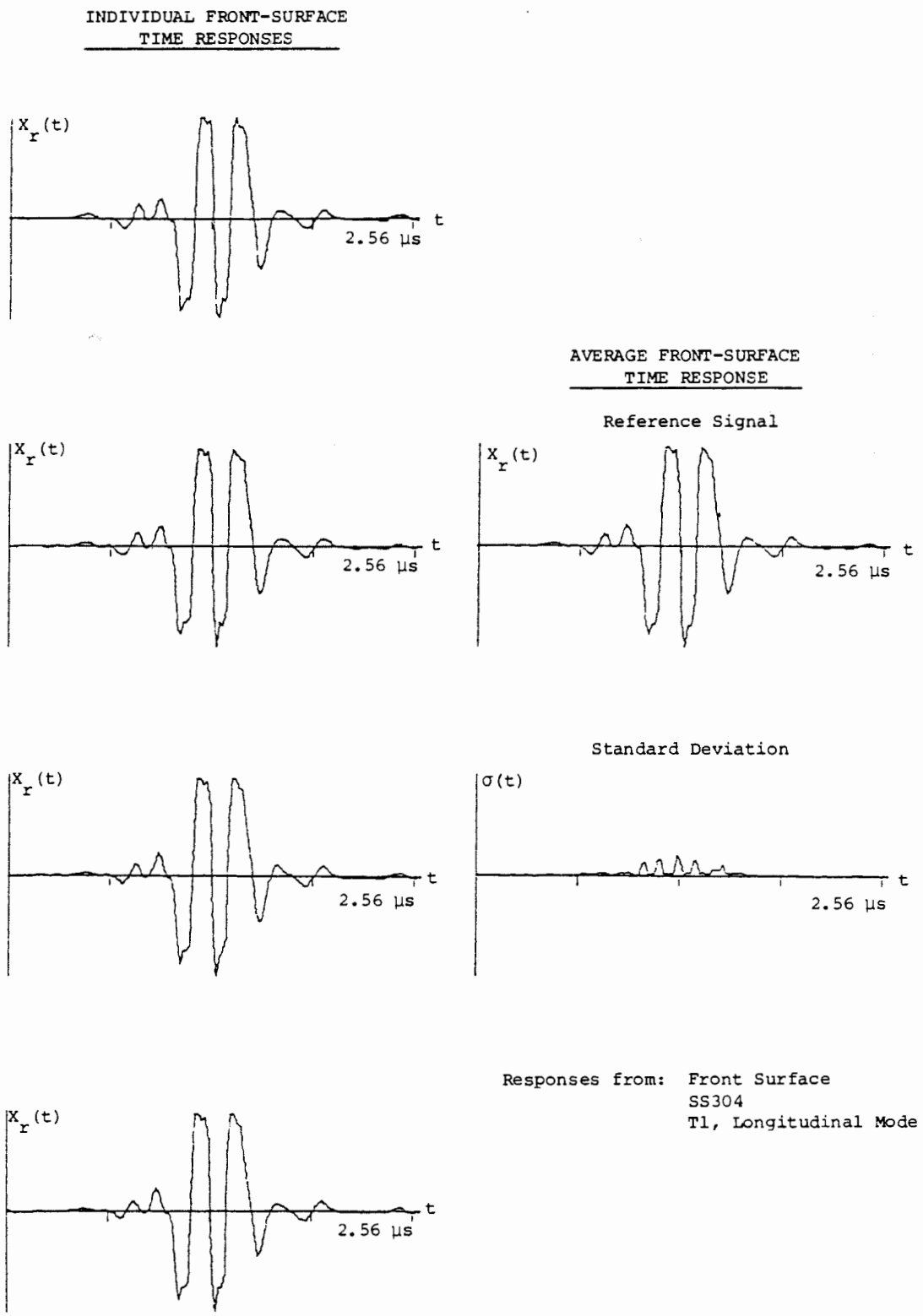

Fig. 3. Four individual front-surface time responses, the average, and the standard deviation [experimental data described in ref. (1)].

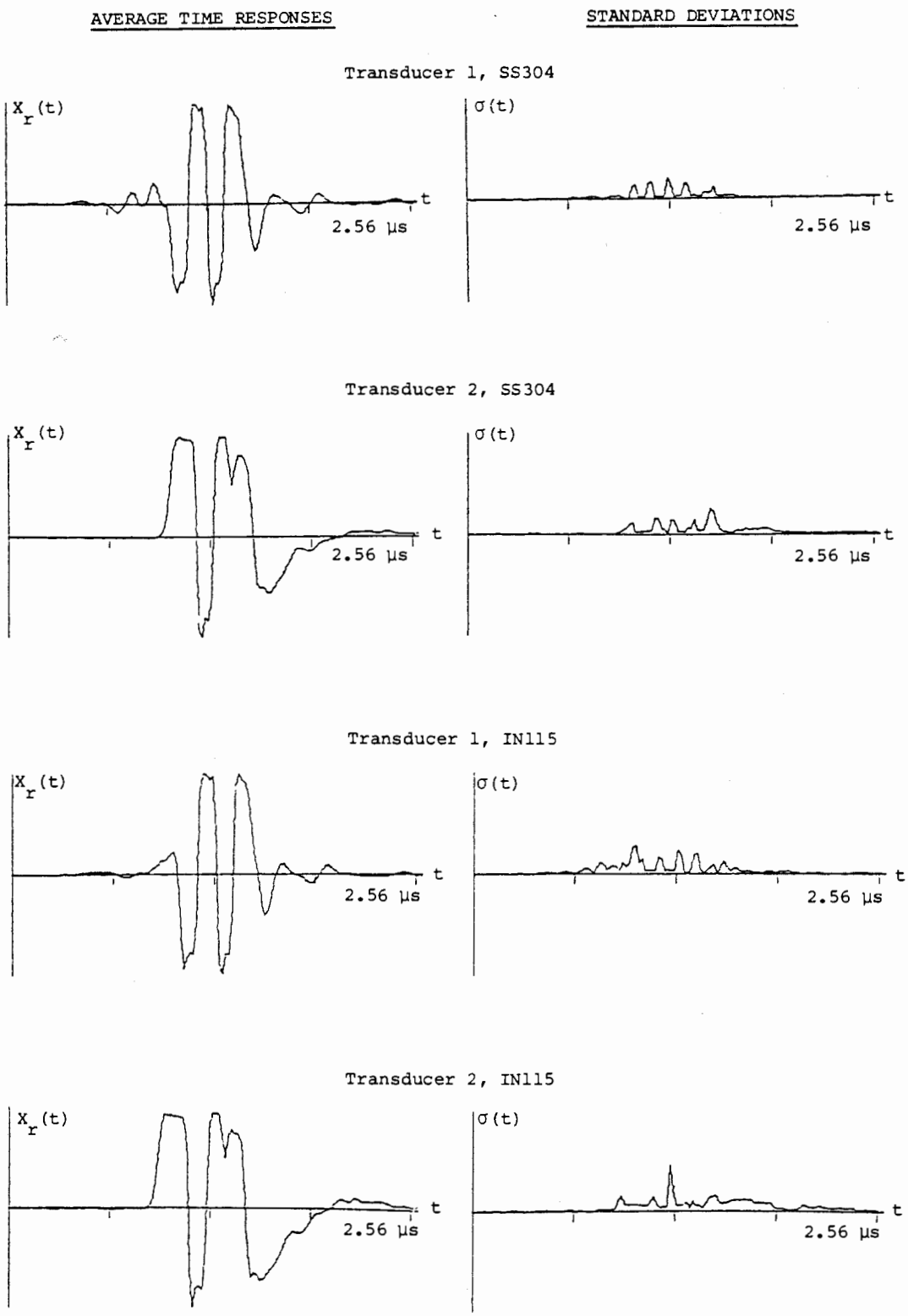

Fig. 4. The average front-surface reference time responses and standard deviations for two transducers and two materials.

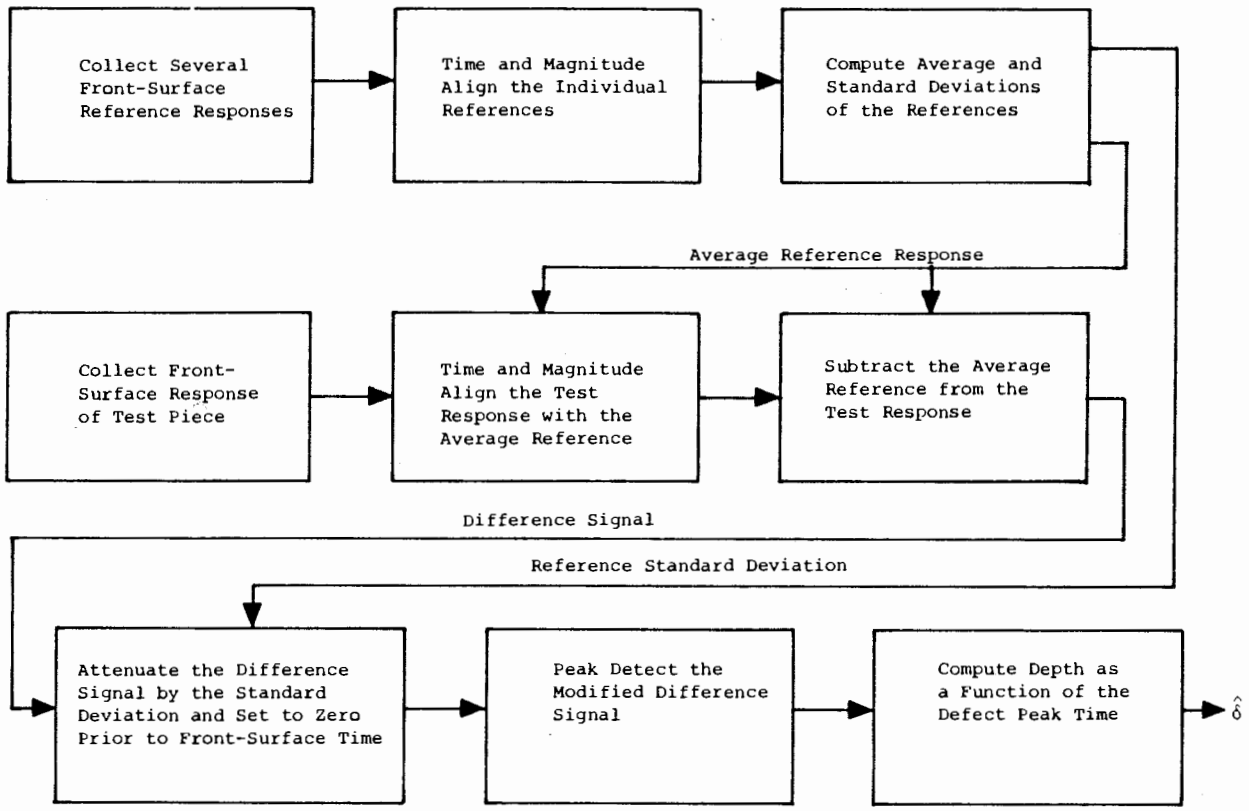

Fig. 5. Block diagram of near-surface defect depth estimation procedure.

the reference standard deviation. The system attenuation function used in this work was

$$w_\sigma(t)=\frac{|d(t)|}{|d(t)|+\sigma(t-\hat{t}_s)} \tag{51}$$

The weighting function is small when the standard deviation is large, and it approaches unity when the standard deviation is small.

If Eq. (51) is substituted into Eq. (50) and rearranged, an alternative interpretation arises:

$$d'(t)=d(t)-d(t)\frac{\sigma(t-\hat{t}_s)}{|d(t)|-\sigma(t-\hat{t}_s)} \tag{52}$$

In this form the modified difference signal may be viewed as equal to the original difference less a percentage of the original difference, where the percentage subtracted out is small if σ is small and large if σ is large. Also, since it is known that the defect does not exist above the surface, any difference signal prior to $t=0$ is known not to result from the defect, so $d'(t-\hat{t}_s)$ is also set to zero for all t less than $\hat{t}_s$:

$$d'(t-\hat{t}_s)=0 \qquad (t<\hat{t}_s) \tag{53}$$

The peak detection algorithm is used on the modified difference signal $d'(t)$ to find the defect occurrence time estimate $\hat{t}_d$. A block diagram of the depth estimation method is shown in Fig. 5.

SIMULATION RESULTS

The time domain solution for the estimation of near-surface defect depths was programmed and evaluated on 24 pulse-echo longitudinal shots of defects less than 0.13 in. deep. The 24 defects were all side-drilled holes. The peak detector acquired the defect signal within the residual front-surface noise 22 out of the 24 times, and the depth estimation produced a mean absolute depth error of 0.015 in. With respect to the total 0.130-in. range, the average error was 12%, and with respect to the true defect

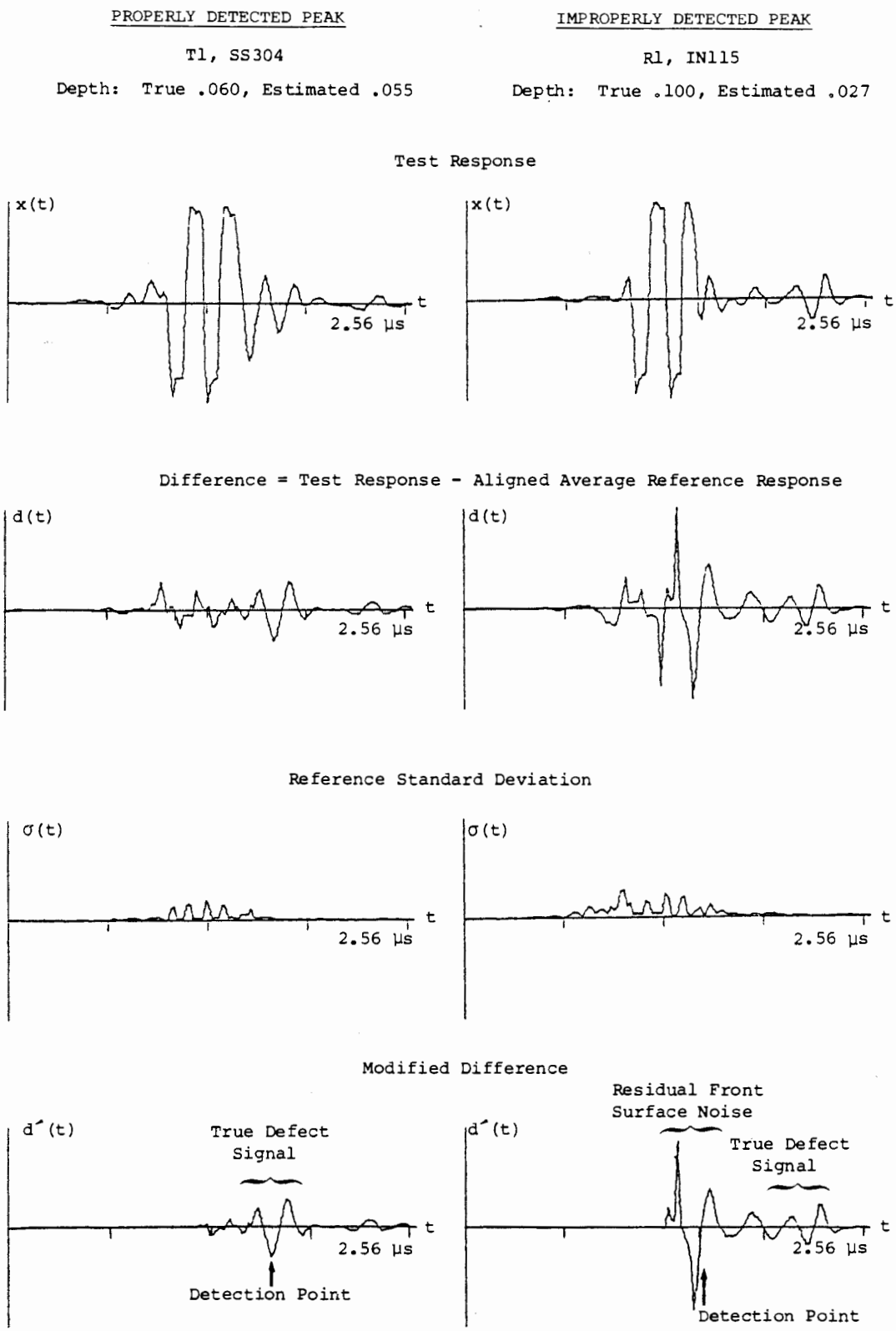

Fig. 6. Examples of processed near-surface defect time signals.

Table I. Summary of Results in Estimating the Depths of Near-Surface Defects[a]

Category	Mean absolute error (in.)	Mean percentage error[c]	Number of waveforms
Overall Data Base[b]	0.015	25%	24
Transducer 1[b]	0.018	30%	12
Transducer 2	0.011	20%	12
Stainless Steel	0.008	13%	12
Inconel[b]	0.021	37%	12

True depth (in.)	Mean estimates depth (in.)	Mean absolute error (in.)	Mean percentage error[c]	Number of waveforms
0.020[b]	0.035	0.015	75%	2
0.040	0.034	0.007	18%	4
0.050	0.038	0.012	24%	2
0.060	0.043	0.017	28%	4
0.080	0.062	0.017	21%	4
0.100[b]	0.082	0.020	20%	4
0.125	0.112	0.013	10%	4

[a] From ref. (1).
[b] Data includes peak detection errors in acquiring the defect signal.
[c] Percentage error is in terms of true defect depth.

depths, the average percentage error was 25%. These results are tabulated in Table I along with a more detailed breakdown of error according to transducer, material type, and true defect depth.

The two cases where the peak detector missed the defects and acquired spurious noise spikes were the transducer 1 shots of the 0.020- and 0.100-in. deep holes in Inconel. The resulting depth estimates were 0.041 and 0.027 in., respectively, giving errors of 105% and 73%. These errors adversely affect the T1 and Inconel results, as seen in Table I, and explain most of the performance variation between transducers and metals. Representative examples of the time responses for correctly and incorrectly acquired signals are shown in Fig. 6.

CONCLUSIONS

The time domain algorithm has been shown to yield good estimates of defect depth as well as to recover the defect signal from the overlapped front-surface response. The authors are currently developing a joint time and frequency domain solution that combines the best features of each and, also, provides for more than one iteration, as discussed above. This combined algorithm will be reported in a future paper. Both algorithms can be implemented in a computer to provide a signal processing basis for automatic processing.

ACKNOWLEDGMENT

This work was supported in part by the General Electric Company, Aircraft Engine Group, under Purchase Order No. 200-4S2-14N46536.

REFERENCES

1. D. Cleveland, A. R. Barron, and A. N. Mucciardi, *Continued Analysis of Digitized Ultrasonic Echo Waveforms Using Adaptive Learning Network Techniques: Phase II-ALN Classifier to Detect and Discriminate Between Near- and Far-Surface Defects in Engine Turbine Disks*, Adaptronics, Inc., Final Technical Report to GE-Aircraft Engine Group, Evendale, OH, under Contract No. 200-4S2-14N46536 (January 1979).
2. D. Cleveland, and A. N. Mucciardi, Frequency domain methods for reducing transducer variability, *J. Nondestructive Eval.* 1(2): to appear (1980).
3. D. Cleveland, A. R. Barron, and A. N. Mucciardi, Ultrasonic waveform features that discriminate between two- and three-dimensional reflectors, in preparation.
4. C. M. Elias, and T. J. Moran, A pseudorandom binary noise ultrasonic system, *Proc. ARPA/AFML Rev. Progr. Quantitative NDE*, AFML-TR-78-205 (January 1979), pp. 511–521.
5. M. H. Loew, R. Shankar, and A. N. Mucciardi, Experiments with echo detection in the presence of noise, using the power cepstrum and a modification, *Proc. IEEE Int. Conf. Acoustics, Speech, and Signal Processing*, Hartford, CT, (May 1977).
6. R. Shankar and A. N. Mucciardi, Near-surface defect detection, to appear in *Materials Evaluation*.
7. R. Shankar, and R. N. McDonaugh, The phase cepstrum and its applications to ultrasonic testing, *Proc. 1978 IEEE Int. Conf. Acoustics, Speech, and Signal Processing*, Tulsa, OK (April, 1978).
8. J. Tiemann and J. D. Young, Ultrasonic inspection system with high near-surface detectability, *Proc. ARPA/AFML Rev. Progr. Quantitative NDE*, AFML-TR-78-205 (January 1979), p. 54.
9. B. R. Tittman, O. Buck, and L. Ahlbey, Surface wave scattering from elliptical cracks for failure prediction, *Proc. ARPA/AFML Rev. Progr. Quantitative NDE*, AFML-TR-78-205 (January 1979), pp. 511–522.

APPENDIX: LOCATION OF SIGNALS THROUGH CENTER OF MASS TECHNIQUES

When processing waveforms, it is often desirable to establish the time of occurrence for a signal of interest. The information may be useful to determine the time of one event with respect to another or to set the parameters of a time window so that the signal may be centered and isolated before further

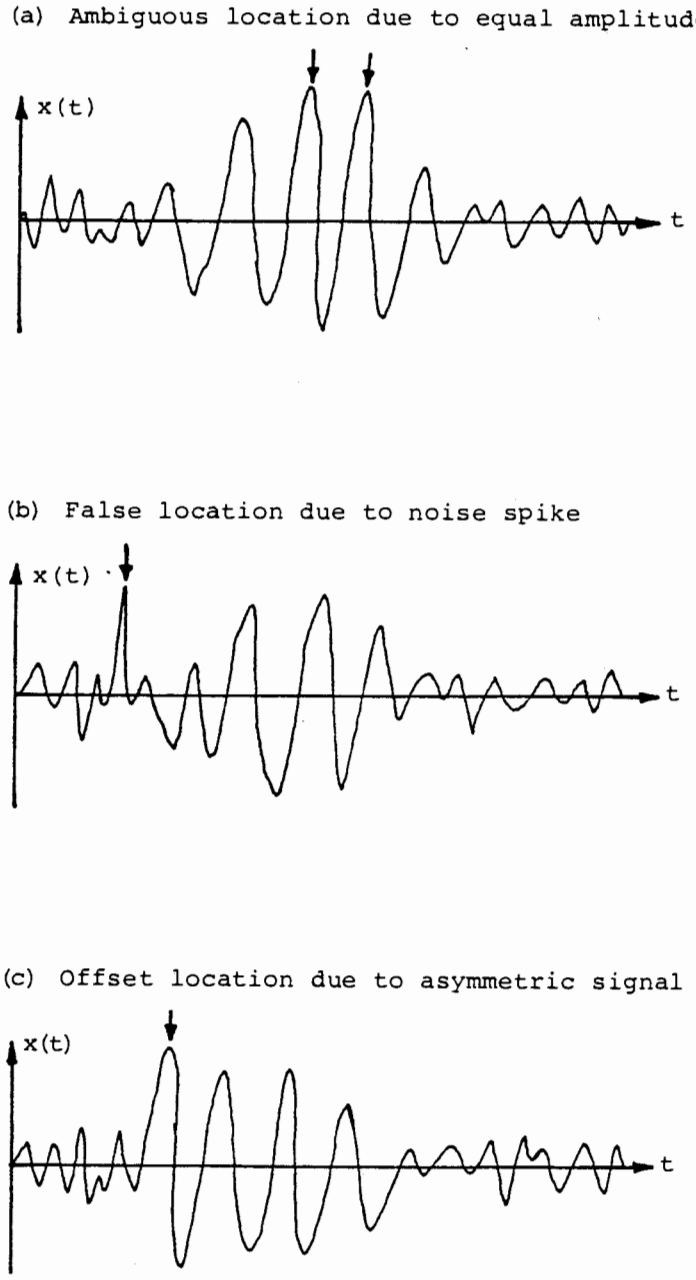

Fig. A1. Disadvantages of peak detection methods for signal location.

processing. A procedure is discussed here for locating signals through center-of-mass techniques. It is assumed (a) that the duration of a signal is limited and known within a factor of two or three, and (b) that the existence of the signal may be adequately recognized by its amplitude, which is greater than the surrounding noise. No other attempt is made here to distinguish between signal and noise.

A common approach to signal location is peak detection; the time at which the waveform reaches its maximum amplitude is defined to be the signal center. For oscillatory signals, such as exist in ultrasonics, this method can produce highly inconsistent results for two reasons. First, as shown in Fig. A1(a), if two peaks have the same or very nearly the same amplitude, there is ambiguity as to the location time.

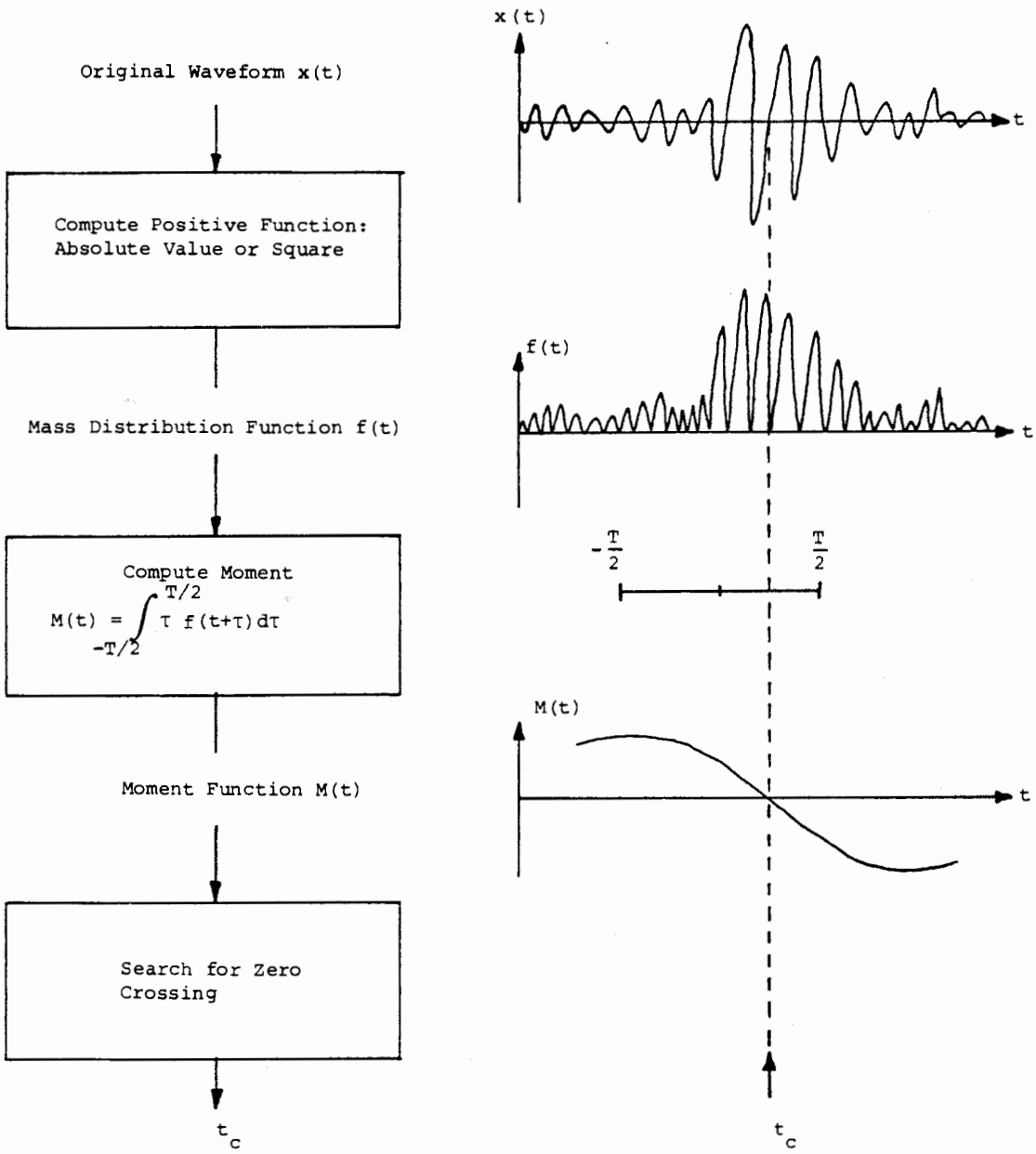

Fig. A2. Procedure for finding signal center of mass.

In two experimentally identical waveforms, the relative peak amplitudes may shift infinitesimally, but the occurrence times would shift dramatically. Second, as shown in Fig. A1(b), the existence of a noise spike which happened to peak above the signal would totally disrupt the results. Another disadvantage of peak detection arises with asymmetric signals. As demonstrated in Fig. A1(c), it may be more desirable to define the occurrence time to be at the center of the signal rather than toward the end where the peak amplitude occurred.

The following procedure significantly reduces the above problems. First, the original waveform $x(t)$ is rectified or squared to give an always positive signal $f(t)$, which may be viewed as a mass distribution along the time axis. Next, a window of length T, where T is approximately one to three times the length of the signal, is moved along the waveform.

The center of the signal t_c is defined to be that point in time for which the window, under the mass distribution $f(t)$, balances in the middle. At any point in time, the mass moment $M(t)$ about the center of the window is

$$M(t)=\int_{-T/2}^{+T/2}\tau f(t+\tau)d\tau \qquad \text{(A1)}$$

where τ is the time distance from a mass point to the center of the window. If the window is to the left of the signal, the predominance of the signal mass is in the right half of the window and the moment $M(t)$ will be positive. Similarly, when the window is to the right of the signal, $M(t)$ is negative. At the signal center, or the balance point, $M(t)$ is zero. Thus the signal center t_c is found by searching the moment curve $M(t)$ for the zero crossing point. The procedure is illustrated in Fig. A2.